THE JOURNAL OF PHYSICAL CHEMISTRY C

Article

pubs.acs.org/JPCC

In-Phase Family and Self-Similarity of Interlayer Vibrational Frequencies in van der Waals Layered Materials

Hui Wang,*[,†] Min Feng,[‡] Xin Zhang,[§] Ping-Heng Tan,[§] and Yufang Wang[‡]

[†]School of Physics and Engineering, Henan University of Science and Technology, Luoyang 471003, China

[‡]Department of Physics, Nankai University, Tianjin 300071, China

[§]State Key Laboratory of Superlattices and Microstructures, Institute of Semiconductors, Chinese Academy of Sciences, Beijing 100083, China

ABSTRACT: We calculated the ultralow frequency of the interlayer shear and breathing modes of van der Waals layered materials by the linear chain model. Some vibrational modes of different layers have exactly the same frequency when only the nearest neighbor interactions are considered, agreeing well with the experimental results of multilayer graphene and MoS_2. These modes are classified as a series of in-phase families based on their eigenvectors. The frequencies of the in-phase family show self-similarity characteristics. When the second nearest neighbor interactions are taken into account, the constant-frequency characteristic of the in-phase family does not hold any more. This means that the in-phase family behavior can be used to determine the sign and strength of the second nearest neighbor interactions unambiguously and conveniently. These results reveal that the in-phase family behavior and the corresponding self-similarity characteristic are robust properties in van der Waals layered materials.

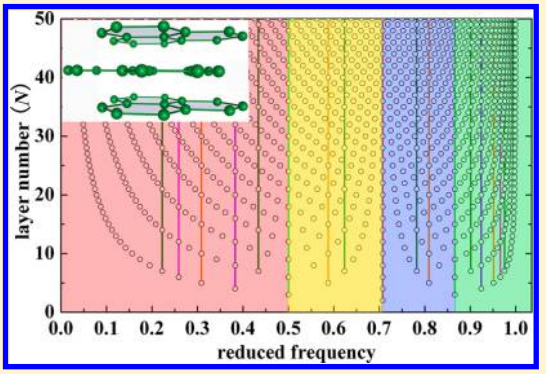

1. INTRODUCTION

Since the discovery of graphene in 2004, its unique properties have stimulated numerous experimental and theoretical studies.[1−3] Soon after, the Raman spectra of graphene on SiO_2 substrate were reported.[4,5] The main spectral features of Raman spectra in multilayer graphene and graphite are the so-called G peak around 1580 cm^{-1} and the 2D band around 2700 cm^{-1}. The 2D band profiles are sensitive to the number of layers.[6,7] By taking the interlayer impact on electronic structure into account, Ferrari et al. successfully explained the 2D band evolution from monolayer graphene to graphite,[4] which makes Raman spectroscopy an unambiguous, high-throughput, and nondestructive characterization tool in the fast-growing field of graphene. In addition to the high-frequency G peak and 2D band, there exists a serial of the ultralow frequency shear mode in multilayer graphene based on the theoretical prediction.[6,8] By combining a high-throughput single monochromator with ultralow-frequency notch filters, the shear mode of each multilayer graphene with the highest frequency was observed.[8] The interlayer breathing modes were also probed in few-layer graphene.[9] Some Raman-inactive shear modes of multilayer graphene can also be resonantly observed in multilayer graphene scrolls.[10]

In addition to multilayer graphene, the interlayer shear and breathing modes are also observed in multilayer MoS_2 and WSe_2.[11−15] Remarkably, the frequencies of low energy modes in multilayer graphene, MoS_2, and WSe_2 can be perfectly fitted by a simple linear chain model with only the nearest neighbor interactions.[6,8−10,15] This suggests that the interlayer frictional characteristics of these excellent lubricants are independent of their layer numbers. Furthermore, the interlayer shear and breathing modes are also observed in other layered bulk materials, such as As_2S_3, As_2Se_3, GaS, and GaSe.[16] Besides the above-mentioned materials, two-dimensional layered crystals can be obtained in group IV elements, III−V binary compounds, transition-metal dichalcogenides, transition-metal oxides, etc.[17−20] The interlayer shear and breathing modes are also expected in them.

In principle, vibrational modes observed in experiments must obey the selection rule. Consequently, some vibrational modes are silent. However, the edge of crystal can relax the selection rule by loss of translational symmetry. This symmetry breaking turns some inactive modes into active ones. For example, the Raman-inactive B_{2g} mode at 867 cm^{-1} was observed at the edge plane of graphite,[21] and the Raman-inactive shear modes of three- to four-layer graphene were also observed in scrolled structures at edges.[10] Therefore, the interlayer shear and breathing modes give a direct fingerprint of layered structures and provide a direct probe of the strength of the interlayer van der Waals interaction.[8]

Family behavior is not a rare phenomenon in low-dimensional materials. The calculated optical transition energies and resonant Raman intensities of single-wall carbon nanotubes show $2n + m$ = constant family behavior.[22−24] The

Received: January 20, 2015
Revised: February 28, 2015
Published: March 4, 2015

DOI: 10.1021/acs.jpcc.5b00608
J. Phys. Chem. C 2015, 119, 6906−6911

calculated vibrational frequencies of C, BN, and BC_3 nanotubes display $n + m$ = constant family behavior.[25,26] Raman spectra show that mod$(n - m, 3) = 2$ semiconducting carbon nanotubes generally have greater Raman scattering intensity than their counterparts mod$(n - m, 3) = 1$.[27] In this paper, we use a linear chain model to deal with general vibrational modes of layered materials and find in-phase family and self-similarity in the interlayer vibrational frequencies.

2. CALCULATION MODEL AND METHOD

We consider the simple linear chain model accompanied by the force-constant method to investigate the interlayer shear and breathing modes of layered materials (Figure 1). The empirical force-constant method has been widely used to calculate the phonon dispersions of graphene, BN, BC_3, nanotubes, etc.[6,25,28,29] The linear chain model accompanied by the interatomic stretching and shear force constants has previously been used to explain the vibrational frequency of epitaxial thin films and the shear and breathing modes of multilayer graphene, MoS_2, and WSe_2.[8,10,13−15,30] As shown in Figure 1, regardless of the detailed structures, multilayer MoS_2 and graphene can be reduced to the linear chain model if only the interlayer shear and breathing modes are concerned. For N layer structures, there are three acoustic modes, $2(N - 1)$ in-plane shear modes and $N - 1$ breathing modes. The interlayer vibrational modes can be computed by diagonalizing the corresponding $3N \times 3N$ dynamical matrix.

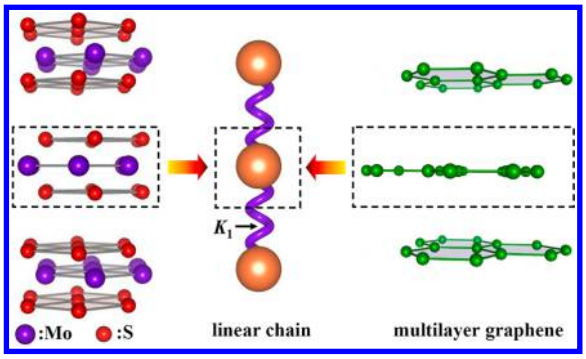

Figure 1. Structure of the multilayer MoS_2 (left), multilayer graphene (right), and the linear chain model (middle). K_1 represents the nearest neighbor interaction.

3. CALCULATED RESULTS AND DISCUSSION

3.1. Nearest Neighbor Interaction. As in multilayer graphene, MoS_2, and WSe_2,[8,10,14,15] only the nearest neighbor interaction is taken into account, and farther interactions are neglected in this section. Under these conditions, there are three force constants for the breathing mode: two tangential force constants K_1^x and K_1^y (in-plane constant) for the shear mode and one radial force constant K_1^z (out-of-plane constant). By diagonalizing the dynamical matrix, the frequency $\omega_i(N)$ of the ith vibrational mode in N layers structure is given by

$$\omega_i^{x/y/z}(N) = \omega_{\max}^{x/y/z} \sin\left(\frac{i-1}{2N}\pi\right) \tag{1}$$

$$\omega_{\max}^{x/y/z} = \frac{1}{\pi c}\sqrt{\frac{K_1^{x/y/z}}{\rho}} \tag{2}$$

where $i = 1, 2, ..., N$, c is the speed of light, ρ is the single-layer mass per unit area, and N is the total number of layers. Therefore, $\omega_N(N)$ is the highest frequency mode and $\omega_1(N)$ is the lowest one. The corresponding displacement eigenvector $e_{i,j}(N)$ of the jth layer in the ith mode is given by

$$e_{i,j}^{x/y/z}(N) = \cos\left[\frac{(i-1)(2j-1)}{2N}\pi\right] \tag{3}$$

For $i = 1$, $\omega_1^{x/y/z}(N) = 0$, and every component of the eigenvector is the same. Obviously, it is the translational mode along x, y, or z direction. For $i = 2, 3, ..., N$, the above equations give the frequencies and eigenvectors of the $3(N - 1)$ optical modes. The frequencies of optical modes reach the minimum $\omega_2^{x/y/z}(\infty) \to 0$ $(i = 2, N \to \infty)$ and maximum $\omega_N^{x/y/z}(\infty) = \omega_{\max}^{x/y/z}(i = N, N \to \infty)$.

The frequency $\omega_i(N)$ is dependent on the magnitude of the force constant. This means shear and breathing modes have different frequency $\omega_i(N)$. To manifest their common character, we define the reduced vibrational frequency $\omega_i^R(N)$,[30] which is independent of the magnitude of the nearest neighbor force constant.

$$\omega_i^R(N) = \frac{\omega_i^{x/y/z}(N)}{\omega_{\max}^{x/y/z}} = \sin\left(\frac{i-1}{2N}\pi\right) \tag{4}$$

It is clear that the reduced frequency $\omega_i^R(N)$ has no relationship with the nearest neighbor force constant $K_1^{x/y/z}$. Furthermore, the reduced frequencies of the interlayer shear

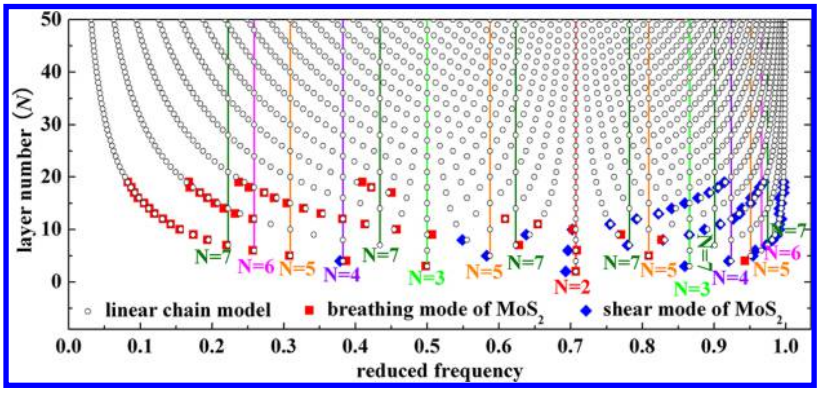

Figure 2. Reduced frequencies of different layer numbers. The vertical lines mark the vibrational mode with the same frequency. The calculated results (○) agree well with the experimental data of MoS_2 (■ and ◆).[14] Some layer numbers of the lowest frequencies marked by the vertical lines are labeled.

DOI: 10.1021/acs.jpcc.5b00608
J. Phys. Chem. C 2015, 119, 6906−6911

and breathing modes have exactly the same evolutions with layer numbers. Therefore, we only discuss the reduced frequency $\omega_i^R(N)$ from now on, instead of the frequency $\omega_i^{x/y/z}(N)$.

The calculated reduced frequencies are given in Figure 2, compared with the experimental results of multilayer MoS_2.[14] It is clear that the calculated reduced frequencies agree well with the Raman shifts of the breathing mode of MoS_2. For few-layer MoS_2, the experimentally measured frequencies of shear mode are a little smaller than the calculated results. For example, the measured frequency of shear mode in bilayer MoS_2 (22.6 cm^{-1}) is 0.5 cm^{-1} lower than the calculated one. It is within the experimental error range. Therefore, the frequencies of the shear and breathing modes of MoS_2 match the linear chain model very well.

In Figure 2, the vibrational modes with exactly the same frequencies are marked by the vertical lines. For example, according to eq 4, the reduced frequency $\omega_i^R(N)$ of bilayer is $\omega_2^R(2) = \sin(\pi/4)$. For even layer numbers, $\omega_{N/2+1}^R(N) = \sin(\pi/4)$ if $i = N/2 + 1$. Therefore, the ith mode of N layers (N is even and $i = N/2 + 1$) have exactly the same frequency and are located on the vertical line of $N = 2$ in Figure 2. Generally, the ith mode of N layers has exactly the same frequency with the $(m \times i - m + 1)$th mode of $m \times N$ layers ($m = 2, 3, 4, ...$).

Why do these modes have exactly the same frequencies? To reveal the mechanism, we depict some vibrational modes in Figure 3. For the vibrational mode of bilayer with the reduced

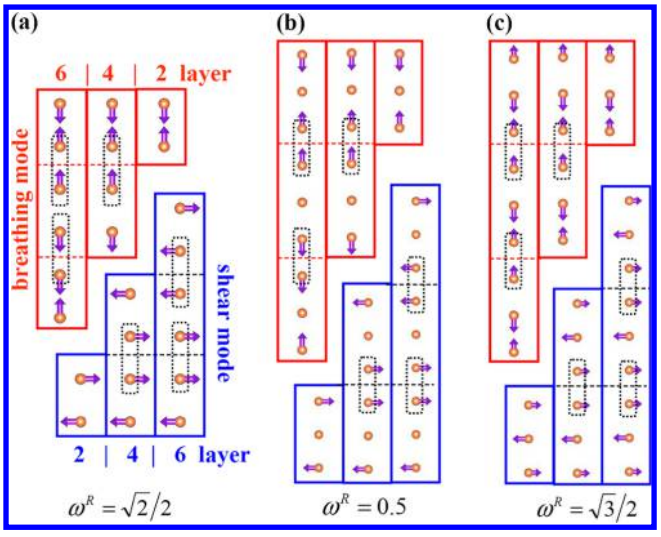

Figure 3. Interlayer shear and breathing modes of in-phase family. Reduced frequencies ω^R are labeled at the bottom. Two atoms enclosed by the dashed rectangle move in phase with each other.

frequency $\omega_2^R(2) = \sqrt{2}/2$, the upper and lower layers move out of phase with each other (Figure 3a). The breathing and shear modes of four layers are very similar to their corresponding modes of bilayer. However, the second and the third layers move in phase, not out of phase, with each other. This means the spring connecting the second and the third layer has no contribution to this vibration. A similar condition occurs in the vibrational modes of six layers: the second (fourth) and the third (fifth) layer move in the same direction with the same amplitude. Consequently, the spring connecting the second (fourth) and the third (fifth) layer does not function at all. As we only take the nearest neighbor interaction into account, the vibrational modes of four (six) layers in Figure 3a can be viewed as a vibration of two (three) independent bilayers. This is why these vibrational modes have exactly the same frequency.

The shear and breathing modes of the lowest frequency in triple layers are depicted in Figure 3b. The upper and lower layers move in opposite directions, while the middle layer remains motionless. In six layers, the third and the fourth layers move in phase with each other. When it comes to nine layers of Figure 3b, the third (sixth) and the fourth (seventh) layers move in phase with each other, as well. The vibrational modes of six (nine) layers in Figure 3b can be viewed as two (three) independent triple layers. Consequently, the vibrational modes in Figure 3b have the same frequency.

The vibrational modes of the highest frequency in triple layer are shown in Figure 3c. The upper and lower layers move in the same direction, while the middle layer moves in the opposite direction. So as to keep the mass center, the amplitude of the middle layer is two times as large as that of other layers. In six layers, the third and the fourth layer have not only the same movement direction but also the same amplitude. Similar conditions also occur in the third (sixth) and the fourth (seventh) layer of nine layers. Therefore, their vibrational frequencies are equal. As in the previous discussion about Figure 3a–c, two atoms enclosed by the dashed rectangle move in phase with each other. Therefore, these modes are named as the in-phase family. On the basis of their eigenvectors, the vibrational modes marked by the vertical lines in Figure 2 belong to the in-phase family.

Self-similarity is found in the vibrational frequencies of Figure 2. As shown in Figure 4a, the reduced frequencies can be divided into two parts: lower and higher than $1/2^{0.5}$. We amplify the low- and high-frequency parts in the left and right sides of Figure 4, respectively. The horizontal axis ranges of Figure 4b, c, and d are 0–0.705, 0–0.495, and 0–0.38, respectively. Although their horizontal axes are getting narrower, Figure 4b–d look similar to each other. In Figure 4a, the lowest frequency originates from the bilayer vibration ($N = 2$). In Figure 4b, c, and d, their lowest frequencies come from $N = 3$, 4, and 5, respectively. Similar conditions occur in Figure 4e, f, and g as well. Therefore, it can be clearly seen from Figure 4 that the frequencies of interlayer vibrational modes show self-similarity characteristics.

3.2. Second Nearest Neighbor Interaction. In previous works on layered materials, it was usually assumed that only the nearest neighbor interaction is important, and the interactions between farther layers were neglected.[8−10,15] Although the calculated results based on this simple assumption agree well with experimental data, farther interlayer interactions are not absolutely zero in principle. In order to give a more accurate description, we take not only the nearest neighbor but also the second nearest neighbor interaction into account. Similar to the condition of nearest neighbor interaction, there are three force constants for the second nearest neighbor interaction: K_2^x, K_2^y, and K_2^z. The second nearest neighbor interactions are generally smaller than the nearest neighbor ones. So as to simplify the condition, we assume that all force constants decay with the same rate: $K_2^{x/y/z}/K_1^{x/y/z} = \gamma$. Therefore, we reduce the independent parameters to four (K_1^x, K_1^y, K_1^z, and γ).

The reduced frequencies with $K_2^{x/y/z}/K_1^{x/y/z} = \gamma = 0.1$ are depicted in Figure 5. As marked by the solid lines of Figure 5, the in-phase families are different from those of Figure 2. Every in-phase family in Figure 2 has exactly the same frequency owing to the zero second nearest neighbor interaction. However, the frequencies of in-phase family increase with

DOI: 10.1021/acs.jpcc.5b00608
J. Phys. Chem. C 2015, 119, 6906−6911

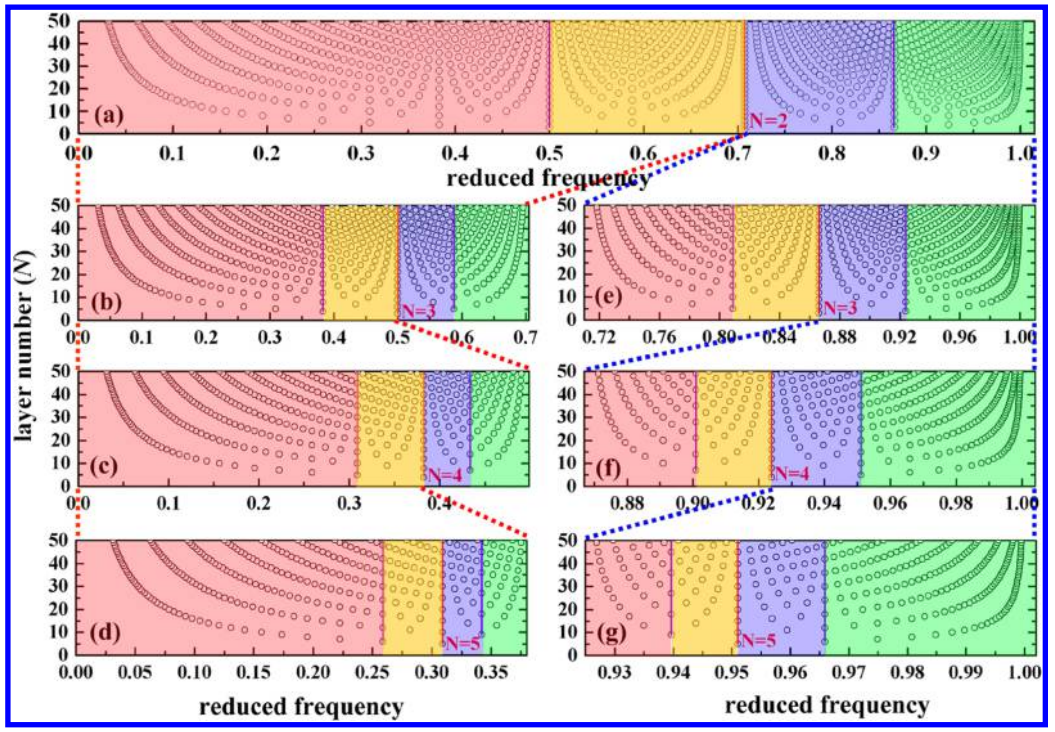

Figure 4. Self-similarity of the interlayer vibrational frequencies. These seven figures look similar to each other, although their horizontal axes are different. The layer numbers of the lowest frequencies are labeled.

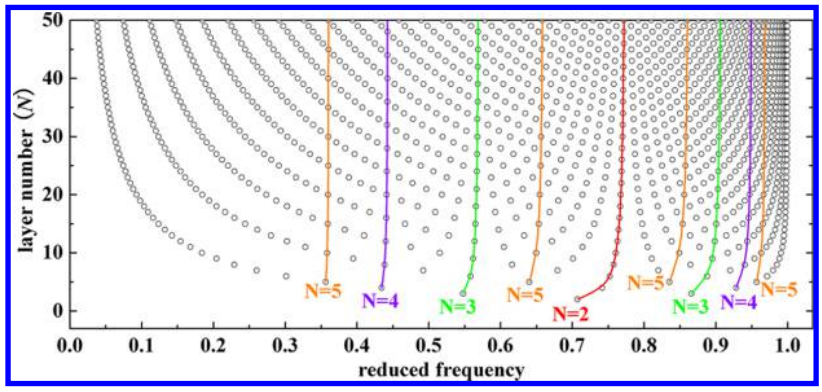

Figure 5. Reduced frequencies with $K_2^{x/y/z}/K_1^{x/y/z} = \gamma = 0.1$. The solid lines mark the in-phase family. Some layer numbers of the lowest frequencies of the in-phase family are labeled.

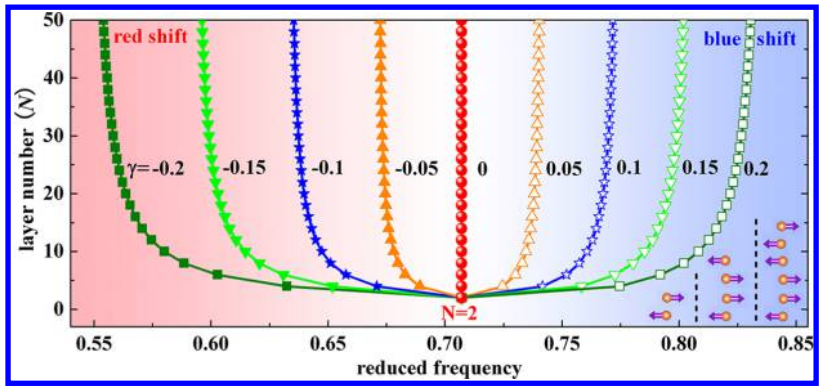

Figure 6. Evolution of reduced frequencies with $K_2^{x/y/z}/K_1^{x/y/z} = \gamma$. Frequency shifts toward either lower frequency (red shift) or higher frequency (blue shift) compared to the $\gamma = 0$ condition. The down-right inset depicts the vibrational modes of two, four, and six layers.

layer number increasing in Figure 5. For example, the reduced vibrational frequencies corresponding to the vibrational modes of Figure 3(a) are 0.707 (bilayer), 0.745 (four layers), and 0.752 (six layers). This frequency increase is originated from

DOI: 10.1021/acs.jpcc.5b00608
J. Phys. Chem. C 2015, 119, 6906−6911

the positive second nearest neighbor force constant.[6,28] As shown in the four-layer vibrational mode of Figure 3a, the first and the third (the second and the fourth) layers move out-of-phase with each other. Therefore, positive force constant between them increases the restoring force and, hence, its vibrational frequency.

It can be clearly seen from Figure 5 that the $N = 2$ in-phase family is the most sensitive one to the second nearest neighbor interaction. Therefore, we investigate its variation with $K_2^{x/y/z}/K_1^{x/y/z} = \gamma$ and show the result in Figure 6. The reduced frequency of bilayer condition ($N = 2$) is $\omega_2^R(2) = \sqrt{2}/2$, which is independent of the second nearest neighbor interaction. On the contrary, the frequencies of other layers are sensitive to γ. Their vibrational frequencies increase (blue shift) when γ is positive and decrease (red shift) when γ is negative. The larger the absolute value of γ is, the bigger the blue or red shift is. Therefore, the $N = 2$ in-phase family can be used to detect the second nearest neighbor interaction.

As shown in Figure 2, both the shear and breathing modes of MoS_2 for $N = 2$ in-phase family agree well with the $\gamma = 0$ condition of Figure 6.[14] The agreement also occurs in mutilayer graphene and WSe_2.[8,10,15] These confirm that the second nearest neighbor interaction can be neglected in these crystals. However, the second nearest neighbor interaction may take effect under special conditions. For example, high pressure will decrease interlayer distance, and in turn, increase the second nearest neighbor interaction. Therefore, this interaction may be amplified and observed under high pressure.

4. CONCLUSION

The linear chain model provides a simple, yet quantitatively reliable, basis for the interlayer vibrational properties of layered materials. Although interlayer shear and breathing modes are quite different from each other, their vibrational frequencies show similar behavior. When only taking the nearest neighbor interaction into account, the ith mode of N layers has exactly the same frequency with the $(m \times i - m + 1)$th mode of $m \times N$ layers ($m = 2, 3, 4, ...$). We name the constant-frequency behavior as in-phase family based on their eigenvectors. When the second nearest neighbor interaction is taken into account, the frequencies of bilayer and bulk material do not change at all. However, other frequencies increase (decrease) with the increase (decrease) of the second nearest neighbor force constant. Therefore, the in-phase family can be used to detect the sign and strength of the second nearest neighbor interaction. Furthermore, we find distinct self-similarity characteristic in the frequencies of interlayer vibrational modes. More importantly, the in-phase family behavior and self-similarity characteristic are popular phenomenon in layered materials.

AUTHOR INFORMATION

Corresponding Author

*E-mail: nkxirainbow@gmail.com.

Notes

The authors declare no competing financial interest.

ACKNOWLEDGMENTS

We are grateful for insightful discussions with Kaien Zhu and Haiyan Gao. This work is supported by the National Natural Science Foundation of China (U1404111, U1404609, 11225421, 11434010, 11474277 and 11404096) and the Young Scientist Foundation of Henan University of Science and Technology (2013QN026). The crystal structure was drawn using the VESTA software.[31]

REFERENCES

(1) Novoselov, K. S.; Geim, A. K.; Morozov, S.; Jiang, D.; Zhang, Y.; Dubonos, S.; Grigorieva, I.; Firsov, A. Electric Field Effect in Atomically Thin Carbon Films. *Science* **2004**, *306*, 666−669.

(2) Bonini, N.; Lazzeri, M.; Marzari, N.; Mauri, F. Phonon Anharmonicities in Graphite and Graphene. *Phys. Rev. Lett.* **2007**, *99*, 176802.

(3) Neto, A. C.; Guinea, F.; Peres, N.; Novoselov, K. S.; Geim, A. K. The Electronic Properties of Graphene. *Rev. Mod. Phys.* **2009**, *81*, 109.

(4) Ferrari, A. C.; et al. Raman Spectrum of Graphene and Graphene Layers. *Phys. Rev. Lett.* **2006**, *97*, 187401.

(5) Gupta, A.; Chen, G.; Joshi, P.; Tadigadapa, S.; Eklund, P. C. Raman Scattering from High-Frequency Phonons in Supported N-Graphene Layer Films. *Nano Lett.* **2006**, *6*, 2667−73.

(6) Wang, H.; Wang, Y.; Cao, X.; Feng, M.; Lan, G. Vibrational Properties of Graphene and Graphene Layers. *J. Raman Spectrosc.* **2009**, *40*, 1791−1796.

(7) Wang, H.; You, J.; Wang, L.; Feng, M.; Wang, Y. Theory of the Evolution of 2d Band in the Raman Spectra of Monolayer and Bilayer Graphene with Laser Excitation Energy. *J. Raman Spectrosc.* **2010**, *41*, 125.

(8) Tan, P. H.; et al. The Shear Mode of Multilayer Graphene. *Nature Mater.* **2012**, *11*, 294−300.

(9) Lui, C. H.; Heinz, T. F. Measurement of Layer Breathing Mode Vibrations in Few-Layer Graphene. *Phys. Rev. B* **2013**, *87*, 121404.

(10) Tan, P.-H.; Wu, J.-B.; Han, W.-P.; Zhao, W.-J.; Zhang, X.; Wang, H.; Wang, Y.-F. Ultralow-Frequency Shear Modes of 2−4 Layer Graphene Observed in Scroll Structures at Edges. *Phys. Rev. B* **2014**, *89*, 235404.

(11) Zeng, H.; Zhu, B.; Liu, K.; Fan, J.; Cui, X.; Zhang, Q. M. Low-Frequency Raman Modes and Electronic Excitations in Atomically Thin Mos_{2} Films. *Phys. Rev. B* **2012**, *86*, 241301.

(12) Boukhicha, M.; Calandra, M.; Measson, M.-A.; Lancry, O.; Shukla, A. Anharmonic Phonons in Few-Layer Mos_{2}: Raman Spectroscopy of Ultralow Energy Compression and Shear Modes. *Phys. Rev. B* **2013**, *87*, 195316.

(13) Luo, X.; Zhao, Y.; Zhang, J.; Xiong, Q.; Quek, S. Y. Anomalous Frequency Trends in Mos_{2} Thin Films Attributed to Surface Effects. *Phys. Rev. B* **2013**, *88*, 075320.

(14) Zhang, X.; Han, W.; Wu, J.; Milana, S.; Lu, Y.; Li, Q.; Ferrari, A.; Tan, P. Raman Spectroscopy of Shear and Layer Breathing Modes in Multilayer Mos2. *Phys. Rev. B* **2013**, *87*, 115413.

(15) Zhao, Y.; et al. Interlayer Breathing and Shear Modes in Few-Trilayer Mos2 and Wse2. *Nano Lett.* **2013**, *13*, 1007−15.

(16) Zallen, R.; Slade, M. Rigid-Layer Modes in Chalcogenide Crystals. *Phys. Rev. B* **1974**, *9*, 1627−1637.

(17) Şahin, H.; Cahangirov, S.; Topsakal, M.; Bekaroglu, E.; Akturk, E.; Senger, R.; Ciraci, S. Monolayer Honeycomb Structures of Group-Iv Elements and Iii-V Binary Compounds: First-Principles Calculations. *Phys. Rev. B* **2009**, *80*, 155453.

(18) Cahangirov, S.; Topsakal, M.; Aktürk, E.; Şahin, H.; Ciraci, S. Two- and One-Dimensional Honeycomb Structures of Silicon and Germanium. *Phys. Rev. Lett.* **2009**, *102*, 236804.

(19) Ding, Y.; Wang, Y. Density Functional Theory Study of the Silicene-Like Six and Xsi3(X = B, C, N, Al, P) Honeycomb Lattices: The Various Buckled Structures and Versatile Electronic Properties. *J. Phys. Chem. C* **2013**, *117*, 18266−18278.

(20) Xu, M.; Liang, T.; Shi, M.; Chen, H. Graphene-Like Two-Dimensional Materials. *Chem. Rev.* **2013**, *113*, 3766−98.

(21) Kawashima, Y.; Katagiri, G. Observation of the out-of-Plane Mode in the Raman Scattering from the Graphite Edge Plane. *Phys. Rev. B* **1999**, *59*, 62−64.

(22) Samsonidze, G. G.; Saito, R.; Kobayashi, N.; Grüneis, A.; Jiang, J.; Jorio, A.; Chou, S. G.; Dresselhaus, G.; Dresselhaus, M. S. Family

DOI: 10.1021/acs.jpcc.5b00608
J. Phys. Chem. C 2015, 119, 6906−6911

Behavior of the Optical Transition Energies in Single-Wall Carbon Nanotubes of Smaller Diameters. *Appl. Phys. Lett.* **2004**, *85*, 5703.
(23) Popov, V.; Henrard, L.; Lambin, P. Electron-Phonon and Electron-Photon Interactions and Resonant Raman Scattering from the Radial-Breathing Mode of Single-Walled Carbon Nanotubes. *Phys. Rev. B* **2005**, *72*, 035436.
(24) Popov, V.; Lambin, P. Resonant Raman Intensity of the Totally Symmetric Phonons of Single-Walled Carbon Nanotubes. *Phys. Rev. B* **2006**, *73*, 165425.
(25) Wang, H.; Cao, X.; Feng, M.; Wang, Y.; Jin, Q.; Ding, D.; Lan, G. Family Behaviour of Raman-Active Phonon Frequencies of Single-Wall Nanotubes of C, Bn and Bc3. *Spectrochim. Acta Part A* **2009**, *71*, 1932−7.
(26) Popov, V.; Lambin, P. Radius and Chirality Dependence of the Radial Breathing Mode and the G-Band Phonon Modes of Single-Walled Carbon Nanotubes. *Phys. Rev. B* **2006**, *73*, 085407.
(27) Heller, D. A.; Barone, P. W.; Usrey, M. L.; Strano, M. S.; Doorn, S. K. Resonant Raman Excitation Profiles of Individually Dispersed Single Walled Carbon Nanotubes in Solution. *Appl. Physics A: Mater. Sci. Process.* **2004**, *78*, 1147−1155.
(28) Mohr, M.; Maultzsch, J.; Dobardžić, E.; Reich, S.; Milošević, I.; Damnjanović, M.; Bosak, A.; Krisch, M.; Thomsen, C. Phonon Dispersion of Graphite by Inelastic X-Ray Scattering. *Phys. Rev. B* **2007**, *76*, 035439.
(29) Wang, H.; Wang, L.; Wang, Y.; Cao, X.; Feng, M.; Jin, Q.; Ding, D.; Lan, G. Vibrational Properties of Single-Wall Bc3 Nanotubes. *J. Phys. Chem. Solids* **2009**, *70*, 8−14.
(30) Luo, N.; Ruggerone, P.; Toennies, J. Theory of Surface Vibrations in Epitaxial Thin Films. *Phys. Rev. B* **1996**, *54*, 5051−5063.
(31) Momma, K.; Izumi, F. Vesta 3for Three-Dimensional Visualization of Crystal, Volumetric and Morphology Data. *J. Appl. Crystallogr.* **2011**, *44*, 1272−1276.

DOI: 10.1021/acs.jpcc.5b00608
J. Phys. Chem. C 2015, 119, 6906−6911